

See discussions, stats, and author profiles for this publication at: <https://www.researchgate.net/publication/279808417>

Influence of temperature on the Rotameric Forms of Propyl Acetate Molecule: Raman, FTIR Spectroscopic Studies Aided by Ab Initio and Car-Parrinello Molecular Dynamics Simulations

ARTICLE *in* THE JOURNAL OF PHYSICAL CHEMISTRY A · JULY 2015

Impact Factor: 2.69 · DOI: 10.1021/acs.jpca.5b03486 · Source: PubMed

READS

34

3 AUTHORS, INCLUDING:



Bipan Dutta

Sammilani Mahavidyalaya

15 PUBLICATIONS 9 CITATIONS

[SEE PROFILE](#)



Joydeep Chowdhury

Jadavpur University

71 PUBLICATIONS 631 CITATIONS

[SEE PROFILE](#)

Influence of Temperature on the Rotameric Forms of the Propyl Acetate Molecule: Raman and FTIR Spectroscopic Studies Aided by ab Initio and Car–Parrinello Molecular Dynamics Simulations

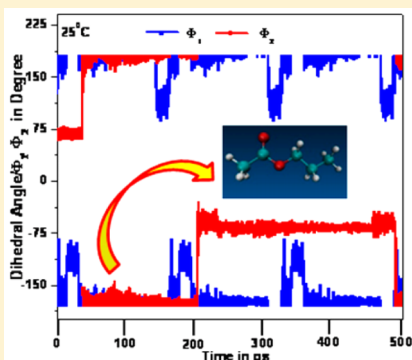
Bipan Dutta,[†] Takeyuki Tanaka,[‡] and Joydeep Chowdhury^{*,†}

[†]Department of Physics, Sammilani Mahavidyalaya, E. M. Bypass, Baghajatin Station, Kolkata 700094, India

[‡]Integrated Centre of Science, Ehime University, 3-5-7 Tarumi, Matsuyama, Ehime 790-8566, Japan

S Supporting Information

ABSTRACT: The conformational preferences of the industrially and biologically significant propyl acetate (PA) molecule have been investigated by Raman and FTIR spectra, aided by ab initio and Car–Parrinello molecular dynamics (CPMD) simulation studies. The PA molecule can exist in various rotameric forms at room temperature, trans-trans [TT], trans-gauche [(TG⁺)/(TG⁻)], gauche-trans [(G⁺T)/(G⁻T)], and gauche-gauche [(G⁺G⁻)/(G⁻G⁺)], depending upon the rotation about the O₃–C₄ and C₄–C₅ bonds of the molecule. The vibrational signatures of different rotameric forms of the PA molecule have been assigned for the first time. Raman and temperature-dependent FTIR spectra of the PA molecule envisage the coexistence of the TT, TG⁺/TG⁻, G⁺T/G⁻T, and G⁺G⁻/G⁻G⁺ forms of the PA molecule at room temperature. However, at low (ca. –95 °C) and high temperatures (ca. 65 °C), the TG⁺ form of the PA molecule is estimated to be preponderant. These results are substantiated by the CPMD simulations, together with the estimation of fwhm values of the vibrational signatures of the PA molecule recorded at high-, room-, and low-temperature domains.



1. INTRODUCTION

Propyl acetate (PA) is an organic ester and is obtained as the product of the esterification reaction between 1-propanol and an acid. It has the characteristic odor of pears and is commonly used in fragrances and in flavor additives.¹ PA is also extensively used for the synthesis of bioactive components such as *cis*- and *trans*-3-(4-propylcyclopent-2-enyl)propyl acetates, which are used as chiral recognitions of moth sex pheromone components.² Due to the enormous biological and industrial applications of the PA molecule, here we report an extensive study on the temperature-dependent IR spectra of the molecule. The Raman spectrum of the molecule in neat liquid at room temperature is also reported herein. The molecule can exist in various rotameric cis, trans, and gauche forms. This paper may be considered as the first comprehensive report concerning the vibrational analyses of the PA molecule in detail, albeit brief analyses of the vibrational signatures (i.e. vibrational frequencies) of the molecule in the crystalline state have been reported elsewhere.³ The preferential existence of various rotameric forms of the PA molecule at high-, room-, and low-temperature domains has also been estimated from experimental observations, aided by ab initio quantum chemical and Car–Parrinello molecular dynamics (CPMD) simulation studies.^{4,5}

2. INSTRUMENTATION

The mid-infrared (IR) spectra of the PA molecule in the liquid state were recorded using a PerkinElmer Spectrum 100 Fourier transform spectrometer equipped with a nichrome wire source, Ge/CsI beam splitter, and DTGS detector. The liquid samples were stored in 12 μm cells attached to KBr windows. Dry nitrogen was purged in the spectrometer chamber to remove traces of atmospheric water vapor. The interferograms were recorded at different temperatures ranging from 65 to –95 °C with four successive scans. The interferograms, so formed, were then transformed through the Blackman–Harris apodization function having a theoretical resolution of 1.0 cm^{–1}.

The temperature-dependent IR studies were carried out in a specially designed cryostat cell made of copper with 4 μm path length, and wedged silicon windows were sealed to the cell with indium gaskets. Thermal resistors made of platinum were used to monitor the temperature, and the cell was cooled by spraying the vapors from the boiling liquid nitrogen. The Fourier transform infrared (FTIR) spectrum of the annealed sample was achieved by heating the cell under vacuum until a temperature of ~65 °C was achieved. The cell was then cooled to room temperature, and the annealed spectrum was recorded.

Received: April 10, 2015

Revised: July 3, 2015

Published: July 4, 2015

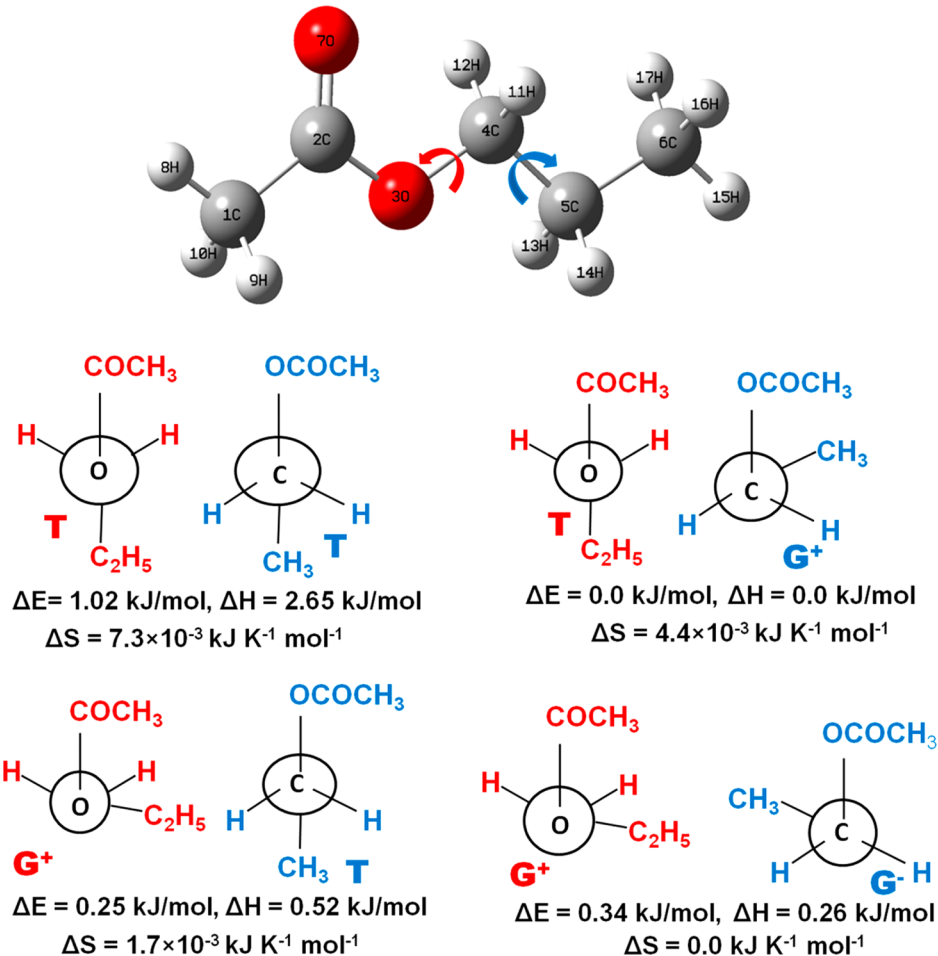


Figure 1. Optimized molecular structures and respective MP2 energies, enthalpies, and entropies of the various rotameric forms of the PA molecule as obtained from the MP2/aug-cc-PVTZ level of theory.

The Raman spectrum of the PA molecule was recorded using a J-Y Horiba confocal triple Raman spectrometer (Model T64000). The sample was excited by a He–Ne laser exciting source emitting at a wavelength of 632.8 nm. The scattered signals were detected with a TE cooled Synapse CCD detector from J-Y Horiba. An Olympus microscope, with two objectives (10× and 50×), was attached. For the experiments, the 10× objective was used to focus the laser beam onto a spot of 2 μm². The laser power at the sample was ~5 mW, and the data acquisition time was 10 s. The holographic grating (1800 grooves/mm) and the slit enabled a spectral resolution of 1 cm⁻¹.

3. THEORETICAL CALCULATIONS

The theoretical calculations were carried out using the Gaussian-09 suite of software.⁶ The self-consistent field (MP2) energies of the TT, TG⁺, G⁺T, and G⁺G⁻ rotameric forms of the PA molecule and vibrational frequencies at their respective optimized geometries were computed at second-order Møller–Plesset (MP2)⁷ levels of theory. The theoretically estimated vibrational frequencies, as obtained from the MP2/aug-cc-pVTZ level of theory, were scaled by the scaling factor 0.94.^{4,8} In the process of geometry optimization for the fully relaxed method using very tight criteria, convergence of all calculations and the absence of imaginary values in the wavenumbers confirmed the attainment of local minima on the potential energy hypersurface. Normal-coordinate analyses

of the various rotameric forms of PA molecules were carried out with the aid of Wilson's GF Matrix method⁹ by extracting the Cartesian force constants from the ab initio MP2 calculations. Local symmetry coordinates were defined as reported elsewhere.¹⁰ The full-width at half maximum (fwhm) values of the vibrational bands were estimated after correcting the baseline of the respective vibrational bands, and the deconvolution of the overlapped bands was performed using the Microcal Origin 08 suite of software. The Gaussian functions were used in the deconvolution procedure.

Ab initio molecular dynamics (MD) simulations have been carried out using the CPMD program¹¹ with the preoptimized TG rotameric form of the PA molecule. In the CPMD approach, the explicit time scale separation concerning the dynamics of fast-moving electrons with respect to the heavy nuclei, as suggested in the Born–Oppenheimer (BO) approximation, was exploited. The hybrid quantum/classical problems were mapped by considering the electronic structures of the PA molecule at successively frozen nuclear frames, leading to the two-component purely classical problem of Lagrangian dynamics. The TG rotameric form of a single PA molecule was placed in a simple cubic box of dimension 10.0 Å. The ab initio MD simulations were then executed in the NVT ensemble at various temperatures (ca. 25, 65, and –95 °C). The length of the CPMD trajectory was set at 4.0 au. The temperature of the ensemble was controlled through a Nose–Hoover thermostat.^{12,13} An electronic fictitious mass parameter

of 700 au was employed in the simulation run. Electronic exchange and correlation have been modeled using a gradient-corrected Perdew, Burke, and Ernzerhof (PBE) functional.¹⁴ Core electrons were treated using the norm-conserving atomic pseudopotentials (PP) of Troullier and Martins,¹⁵ while valence electrons were represented as a plane-wave basis set truncated at an extended energy cutoff of 80 Ry. The simulated data and the respective snapshots were visualized using VMD¹⁶ visualization software.

4. RESULTS AND DISCUSSION

4.1. Molecular Structure. The optimized molecular structures of various rotameric forms of the PA molecule are shown in Figure 1. The relative changes in the MP2 energies (ΔE), enthalpies (ΔH), and entropies (ΔS) of the different rotameric TT, TG^+/TG^- , G^+T/G^-T , and G^+G^-/G^-G^+ forms of the PA molecule are also shown in Figure 1. When the dihedral angles $C_2-O_3-C_4-C_5$ (φ_1) and $O_3-C_4-C_5-C_6$ (φ_2) of the PA molecule are $+60$ and -60° , respectively, the molecule is said to be in the gauche G^+ and G^- forms, respectively. The sign "+" or "-" depends on the direction of clockwise and anticlockwise rotations. G^+T and G^+G^- and their respective enantiomeric forms have nearly equal energies with respect to the most stable TG^+ and its enantiomeric TG^- forms of the PA molecule. The MP2 energy of the TT form of the molecule is ~ 1.02 kJ/mol higher than that of the corresponding TG^+ (TG^-) form. The gauche-gauche G^+G^+ form and its enantiomeric G^-G^- form of the PA molecule can hardly exist in nature, due to the steric hindrance between the methyl and carbonyl groups of the molecule. The probability of the preferential existence of the cis form of the molecule is less in comparison to that of its corresponding trans and gauche forms, as the MP2 energy of the former is ~ 30.01 kJ/mol more than that of the latter.

The selected optimized structural parameters, dipole moments, and rotational constants of the rotameric TT, TG^+ , G^+T , and G^+G^- forms of the PA molecule are shown in Table S1 in the Supporting Information. The O_3-C_4 and C_4-C_5 bond lengths are quite similar for the TT, TG^+ , G^+T , and G^+G^- forms of the PA molecule. Moreover, the skeletal $C_2-O_3-C_4$ and $C_4-C_5-C_6$ bond angles are almost similar for the G^+T , G^+G^- , TG^+ , and G^+G^- forms of the molecule. However, for other forms of the molecule TT, TG^+ and TT, G^+T the bond angles $C_2-O_3-C_4$ and $C_4-C_5-C_6$ are considerably decreased to 114.66 , 114.71° and 110.60 , 110.58° , respectively. Theoretical results further indicate that both the carbon C_1 and C_6 atoms of the $-CH_3$ group of the TT, TG^+ , G^+T , and G^+G^- forms of the PA molecule are approximately sp^3 hybridized, with the relevant bond angles CCH and HCH being ~ 110.29 and 108.61° , respectively.

4.2. Raman and FTIR Spectra of the PA Molecule and Their Vibrational Assignment. The rotameric forms of the PA molecule, as shown in Figure 1, have 17 atoms; hence, 45 fundamental vibrations are associated with each of them. The TT form has C_s point group symmetry, while the TG^+ , G^+T , and G^+G^- forms are in the C_1 point group. The 45 fundamental vibrations of the TT form of the PA molecule with C_s point group symmetry are distributed among A' and A'' symmetry species as

$$\Gamma_{\text{vib}} = 27A' + 18A'' \quad (1)$$

Among these vibrational modes, 27 planar (A') and 18 nonplanar (A'') species are expected to appear in both Raman

and FTIR spectra. However, some of these vibrations, emanating from the TT and the other rotameric TG^+ , G^+T , and G^+G^- forms of the PA molecule, may exhibit degeneracy. The room-temperature (ca. 25°C) Raman and FTIR spectra of the PA molecule in neat liquid are shown in parts a and b of Figure 2, respectively. The theoretically simulated Raman

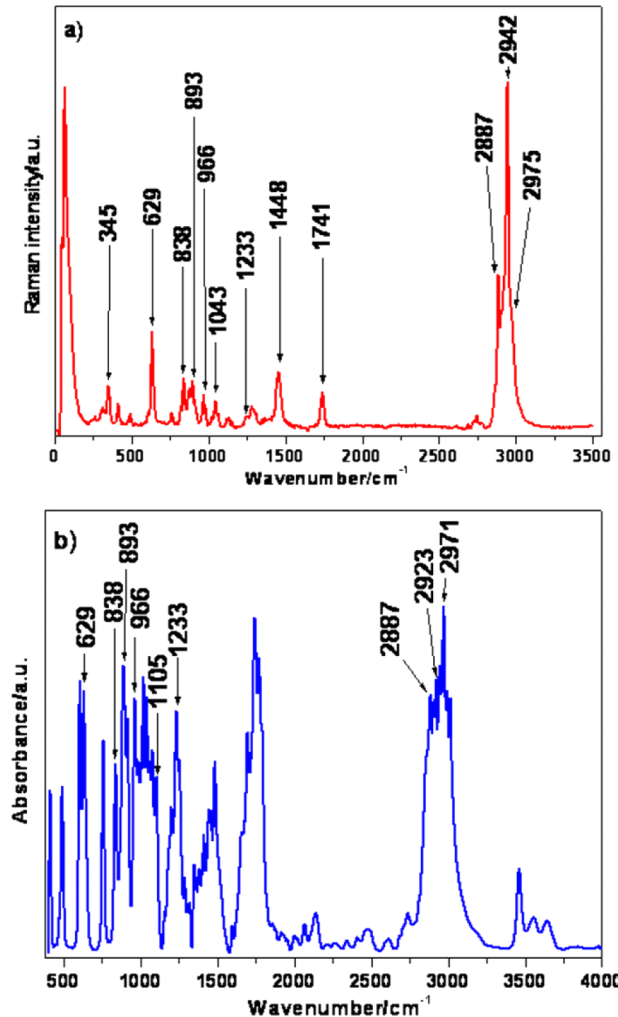


Figure 2. (a) Raman spectrum of the PA molecule in the liquid state recorded in the $50-3500\text{ cm}^{-1}$ region for λ_{exc} 632.8 nm. (b) FTIR spectrum of the PA molecule in the liquid state recorded at room temperature (25°C) in the wavenumber range $400-4000\text{ cm}^{-1}$.

spectra of the TT, TG^- , G^-T , and G^+G^- forms of the molecule and their mixtures are shown in Figure 3. The essential aim of recording the Raman and FTIR spectra is to understand the preferential existence of the rotameric forms of the PA molecule from their respective vibrational signatures. The local symmetries and internal coordinates, so defined, are presented in Table S2 in the Supporting Information. Table 1 gives the experimentally observed FTIR and Raman band frequencies of the PA molecule recorded at room temperature. The theoretically simulated vibrational frequencies of the various rotameric forms of the PA molecule are also shown in Table 1 along with their tentative assignments, as provided from the potential energy distributions (PEDs). The observed disagreement between theory and experiment may arise from the anharmonicity of the potential energy surfaces and may also be due to the general tendency of the quantum chemical

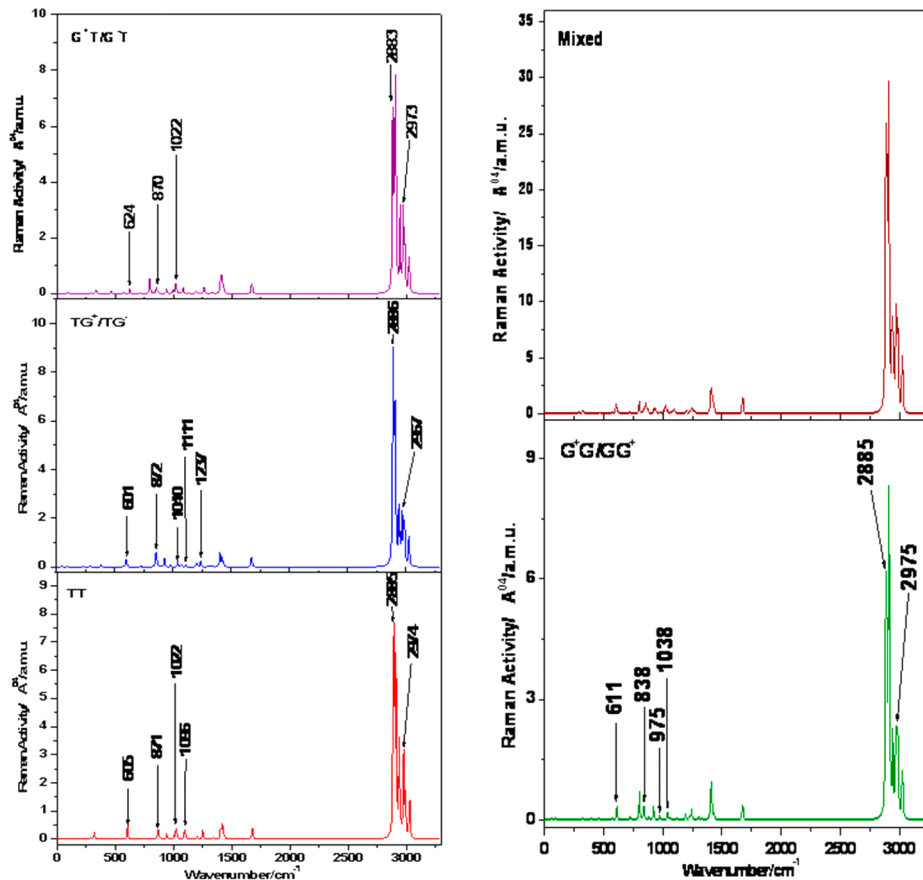


Figure 3. Theoretically simulated gas-phase Raman spectra of the TT, TG^+ (enantiomeric form TG^-), G^+T (enantiomeric form G^-T), and G^+G^- (enantiomeric form G^-G^+) forms and a mixture of all the forms of the PA molecule in the $0\text{--}3500\text{ cm}^{-1}$ region using the MP2/aug-cc-PVTZ level of theory.

methods to overestimate the force constants at the exact equilibrium geometry.^{17–21} Despite this fact, one can see that the positions of the peaks between the experimental and the calculated spectra are in harmony.^{22,23} The intensity profiles showing the differences between the experimentally observed and theoretically simulated Raman bands are shown in Figure S3 of the Supporting Information.

The relative populations of TT, TG^+ , G^+T , and G^+G^- forms are estimated using the relation

$$\frac{[\text{form}_i]}{[\text{form}_j]} = \frac{\sum_i I_i \sum_j A_j}{\sum_j I_j \sum_i A_i} \quad (2)$$

where $\sum_i I_i$ and $\sum_j I_j$ signify the sums of the integrated intensities of the assigned experimental IR bands representing vibrational signatures of i and j conformeric forms of the PA molecule and $\sum_i A_i$ and $\sum_j A_j$ signify the theoretically predicted sums of the absolute intensities of the respective conformeric forms.^{4,24,25}

The relative populations of TT, TG^+ , G^+T , and G^+G^- forms of the PA molecule at room temperature are estimated to be ~21%, 35%, 15%, and 29%, respectively, in accordance with the experimental observations.

The room-temperature FTIR spectrum of the PA molecule in the liquid state (Figure 2b) is characterized by a large number of vibrational signatures; many of them appear as doublets or higher order multiplets in the spectrum. In comparison to FTIR, the Raman spectrum (RS) of the molecule recorded in the liquid state exhibits much fewer, but well-resolved, Lorentzian vibrational signatures. The modes

arising principally from the torsion, stretching, and bending of the aliphatic chain and the twisting, deformation, and rocking vibrations of the externally attached methyl group emanating from various rotameric forms of the PA molecule are identified. In the assignment of the vibrational signatures, the existing, albeit scarce, literature concerning this and related molecules are considered.^{3,4,26} In this connection, it may be mentioned that the calculated frequencies $571\text{--}574$, $452\text{--}457$, and $715\text{--}724\text{ cm}^{-1}$ are given in Table 1, although the corresponding vibrational signatures are not observed experimentally. The intensities of these bands may be too weak to be observed experimentally. The simulated intensities of these bands are also weak, as estimated from the ab initio calculation.

Considerable attention can be drawn concerning the intense bands centered at $\sim 838\text{ cm}^{-1}$ (calculated at 838 cm^{-1} for the G^+G^- form of the PA molecule) and 893 cm^{-1} (calculated 882 cm^{-1} for the G^+G^- form of the PA molecule), 966 cm^{-1} (calculated at 975 cm^{-1} for the G^+G^- form of the PA molecule) in both the Raman and FTIR spectra. The former band has been assigned to $\nu(\text{C-C})$ stretching vibration, while the latter pair has been ascribed to have significant contributions from $\rho(\text{CH}_3)$ rocking vibrations associated with the G^+G^- rotameric form of the PA molecule. The appearances of these vibrational signatures mark the exclusive presence of the G^+G^- form of the PA molecule in the liquid state at room temperature.

Interestingly, the concomitance of the G^+T rotameric form of the molecule in the liquid state is identified from the appearance of a strong Raman band centered at $\sim 345\text{ cm}^{-1}$

Table 1. Observed and Calculated Raman (RS) and FTIR Bands of the PA Molecule for the Various Conformers and Their Tentative Assignments

RS	FTIR	TT (C _s)		TG ⁺ (C _i)		G ⁺ T (C _i)		G ⁺ G (C _i)	
		calcd freq		calcd freq		calcd freq		calcd freq	
		PED%	PED%	PED%	PED%	PED%	PED%	PED%	PED%
48 (vw)		44 (8), S17(8)	S14(54), S8(16), S7(11), S13	40 (7), S17(7)	S14(50), S8(15), S7(10), S13	43 (10), S13(8)	S14(52), S8(16), S7(11), S17	42 (10), S13(8)	S14(52), S8(16), S7(11), S17
65 (vvs)		62 S26(79), S17(8)	S35(56), S17(12), S14(11), S45(5), S26(5)	53 (7), S13(7)	S14(37), S26(26), S8(11), S7	75 S35(68), S16(9), S26(7)	S35(68), S16(9), S26(7)	60	S26(49), S35(28), S14(6)
113 (vw)		82 S22(32), S16(32), S31(23)		90 (5)	S35(48), S17(25), S14(6), S45	91 S26(8), S31(5)	S17(40), S22(23), S14(12), S26(8), S31(5)	92	S17(45), S22(17), S14(14), S35(6)
		127 S22(32), S16(32), S31(23)			100 S26(68), S17(16), S35(6)		S26(68), S17(16), S35(6)	124	S35(30), S26(23), S17(18), S45(13), S16(8)
				159 S16(29), S12(7)	S16(29), S22(27), S45(15), S12(7)			218	S45(71), S17(6)
211 (vvw)		187 S45(91)	S17(62), S35(28), S45(18), S17(48), S35(23), S45(18), S16(39), S16(26), S31(9), S11 (8), S45(39)	178 233	S17(48), S35(23), S45(18), S16(39), S16(26), S31(9), S11 (8), S45(39)	222	S45(86), S16(12), S45(86), S16(12)		244 S31(33), S16(26), S22(12), S11(5), S17(5)
257 (vw)		293 S22(31), S12(9), S29(7)	S31(40), S12(25), S16(8), S20 (6), S11(5) S22(31), S16(21), S11(11), S12(9), S29(7)	291 S45(15)	S31(26), S22(15), S35(15), S45(15)	266 S35(5), S26(5)	S31(54), S22(18), S17(10), S16(43), S12(19), S11(13), S35(5), S26(5)		244 S31(33), S16(26), S22(12), S11(5), S17(5)
309 (w)		320 S345 (s)				292 S12(8)	S16(43), S12(19), S11(13), S35(5), S26(5)		320 S12(33), S31(10), S16(9), S35 (8), S22(8)
				383 S12(55), S31(13), S6(10), S16 (8)		338 S6(5)	S12(31), S22(26), S20(7), S16 (6), S6(5)		400 S12(29), S31(23), S16(14), S6 (6), S26(5)
		408 (s)							400 S12(29), S31(23), S16(14), S6 (6), S26(5)
413 (s)				443 S33(6), S42(5)	S22(28), S31(25), S12(12), S33(6), S42(5)				457 S22(32), S12(14), S31(13), S33(8)
		492 (s)		452 (10)	S12(46), S31(15), S22(13), S6				457 S22(32), S12(14), S31(13), S33(8)
490 (s)						465 S13(61), S8(22)	S12(38), S22(16), S11(9), S6 (9), S31(7)		
607 (sh)		572 605 629 (vs)	S13(68), S8(25), S11(49), S10(26), S16(10)	571 601 629 (vs)	S13(68), S8(25), S11(47), S10(28), S16(7), S12 (6), S20(6)	574 624	S13(61), S8(22) S11(38), S10(21), S16(16), S22(5)		573 611 629 (vs)
692 (vww)		721 760 (345 + 413) ^a (vs)	S33(52), S24(16), S44(15), S25(6), S15(27), S44(11), S10(11), S20(9), S24(9)	722 798	S33(49), S24(19), S44(13), S25(5)	715 798	S33(49), S24(19), S44(13), S15(27), S44(11), S10(11), S20(9), S24(9)		724 802 838
794 (w)									S33(37), S44(20), S24(7), S20 (5), S15(5), S15(24), S44(15), S20(9), S10 (9), S33(7)
838 (vs)									S39(35), S29(32), S24(8)

Table 1. continued

RS	FTIR	TT (C _j)		TG ⁺ (C _i)		G ⁺ T (C _i)		G ⁺ G (C _i)		
		calcd freq	PED%	calcd freq	PED%	calcd freq	PED%	calcd freq	PED%	
873 (vs)	846	S44(32), S24(31), S34(25), S25(7)	848	S39(35), S29(24), S24(14), S10(7)		853	S42(21), S44(14), S24(12), S34(11), S29(10)			
893 (vs)	857	S15(26), S10(18), S29(16), S39(13), S42(8)	857	S20(17), S15(15), S44(13), S16(11), S34(9)		870	S42(15), S44(13), S34(11), S29(10), S15(9)			
909 (sh)	871	S42(31), S20(12), S15(9), S22(9), S16(8)	872	S42(29), S25(7), S32(7), S44(6)		882	S42(26), S24(22), S25(8), S32(8), S44(6)			
	889 (vs)							922	S20(24), S10(20), S6(12), S39(11), S34(5)	
	919 (s)									
				929	S10(27), S20(19), S6(17), S39(11), S42(6)	942	S6(38), S10(20), S20(18)			
				941	S6(37), S10(20), S20(16), S9(5)			975	S6(41), S42(6), S39(6), S29(5)	
				964 (vs)						
	983 (sh)	986 (sh)		980	S6(39), S20(9), S15(8), S42(5)					
				992 (sh)	S39(51), S20(14), S6(12), S29(6)	1000	S39(57), S20(11), S6(10), S29(8)			
				1004	S8(70), S13(18), S7(9)	1008	S8(68), S13(18), S7(9), S20(47), S6(11), S39(10), S29(9)	1008	S8(70), S13(18), S7(9)	
	1012 (sh)	1021 (vs)	1009	1009	S8(70), S13(18), S7(9)	1022	S20(38), S29(24), S39(13), S32(6)	1038	S20(38), S29(24), S39(11), S32(6), S6(5)	
		1022	S20(47), S39(12), S29(11), S6(10)	1040	S20(37), S29(24), S39(13), S32(6)			1060	S39(23), S42(19), S33(9), S44(8), S22(7)	
		1043 (vs)		1043 (vs)						
		1060 (w)		1060 (w)						
				1077 (s)	S42(22), S39(20), S24(9), S22(7), S31(7)	1070	S42(22), S39(20), S24(9), S22(7), S31(7)	1082	S29(37), S42(27), S32(9), S31(8), S22(8)	
				1085 (sh)						
		1105 (s)	1096	S29(35), S42(23), S22(9), S32(9), S31(8)	1111	S24(31), S33(17), S44(15), S29(8), S42(5)	1131	S24(35), S33(27), S44(22)	1118	S24(30), S33(17), S44(15), S42(8), S29(6)
		1126 (w)	1121	S24(39), S33(26), S44(21), S25(7)						
		1151 (w)	1158 (vw)					1194	S15(31), S11(14), S10(13), S23(7), S6(6)	
	1207 (vw)	1201 (w)	1203	S15(40), S11(12), S10(12), S23(9)	1201	S15(30), S25(15), S11(9), S10(9), S23(8)		1191	S15(29), S11(15), S10(13), S23(6), S6(6)	
		1204	S4(6), S25(49), S34(23), S44(12), S33(6)	1206	S25(44), S15(15), S11(5)					
	1233 (s)			1237	S34(64), S25(11), S44(7)	1224	S34(42), S25(20), S44(8), S15(6), S24(5)	1227	S34(63), S44(11), S15(6)	
	1244 (vw)	1249	S34(56), S25(36)					1243	S25(57), S32(9), S15(7), S29(6)	

Table 1. continued

RS	FTIR	TT (C ₃)			TG ⁺ (C ₁)			G ⁺ T (C ₁)			G ⁺ G (C ₁)	
		calcd freq	PED%	calcd freq	PED%	calcd freq	PED%	calcd freq	PED%	calcd freq	PED%	
1281 (s)	1285 (w)	1257	S32(56), S23(21), S42(5)	1300	S32(49), S23(17), S40(12)	1261	S32(57), S23(16), S42(5)	1266	S25(62), S34(26)	1301	S32(55), S25(12), S40(9), S23(6), S29(5)	
1312 (sh)	1312 (vw)	1320	S4(65), S23(11), S10(7), S32(6)	1318	S4(51), S23(16), S32(10), S29(7), S10(5)	1321	S4(68), S23(11), S10(8)	1320	S4(58), S23(20), S10(6)			
1343 (vw)	1352 (w)	1335	S40(84), S39(8)	1331	S40(51), S4(12), S39(9), S32(8), S23(5)	1333	S40(83), S39(8)	1329	S40(49), S4(13), S23(11), S39(6)			
1363 (vw)	1379 (w)	1345	S23(44), S4(12), S32(11), S29(10), S10(5)	1342	S23(36), S40(26), S4(13), S10(6)	1342	S23(54), S32(10), S4(9), S29(6), S40(5)	1343	S23(42), S40(30), S4(8)			
		1402	S5(89), S6(7)	1401	S5(88), S6(7)	1401	S5(89), S6(7)	1401	S5(88), S6(7)	1401	S5(88), S6(7)	
		1410	S7(92), S8(7)	1404	S30(91)	1409	S7(91), S8(7)	1407	S30(86)	1407	S30(86)	
		1418	S30(66), S41(17), S21(12)	1410	S7(92), S8(7)	1413	S21(77), S30(16)	1409	S7(84), S8(6)	1411	S21(79), S43(7)	
				1422	S43(57), S21(26), S41(7), S44(5)	1421	S30(52), S41(30), S21(12)	1429	S43(89), S44(8)	1427	S43(75), S21(8), S44(7)	
				1429	S21(46), S41(45)	1429	S43(89), S44(8)	1432	S41(78), S42(7), S43(6)	1432	S41(78), S42(7), S43(6)	
				1430	S43(90), S44(8)	1434	S21(51), S41(33)	1434	S41(57), S30(8), S42(6)	1432	S41(78), S42(7), S43(6)	
				1440	S21(37), S30(30), S41(25)	1435	S41(43), S43(28), S21(18)	1435	S41(57), S30(8), S42(6)	1432	S41(78), S42(7), S43(6)	
		1448 (vw)	1448 (607 + 838) ^a (s)	14674	S9(79), S10(6)	1674	S9(79), S10(6)	1674	S9(78), S10(6)	1674	S9(78), S10(6)	
		1462 (492 + 964) ^a (s)	1483 (s)									
		1518 (vww)	1594 (w)	1655 (vw)	1674	S9(79), S10(6)	1674	S9(78), S10(6)	1674	S9(78), S10(6)	1674	S9(78), S10(6)
		1678 (vww)	1695 (s)	1744 (vvs)	1774 (889 × 2) ^b (vs)	1774 (889 × 2) ^b (vs)	1774 (889 × 2) ^b (vs)	1774 (889 × 2) ^b (vs)	1774 (889 × 2) ^b (vs)	1774 (889 × 2) ^b (vs)	1774 (889 × 2) ^b (vs)	
		2741 (vww)	2737 (w)	2808 (sh)	2851 (sh)	2884 (s)	2885 (s)	2886 (s)	2883 (s)	2885 (s)	2885 (s)	
		2855 (sh)	2887 (s)	2893 (s)	2893 (s)	2893 (s)	2893 (s)	2892 (s)	2899 (s)	2893 (s)	2893 (s)	
		2905 (s)	2902	2909	2908	2933	2936	2908	2909	2908	2908	
		2923 (s)	2902	2909	2908	2933	2936	2908	2909	2908	2908	
		2944 (ws)	2944 (s)	2944 (s)	2944 (s)	2944 (s)	2944 (s)	2944 (s)	2944 (s)	2944 (s)	2944 (s)	

	RS	FTIR	TT (C ₂)			TG ⁺ (C ₁)			G ⁺ T (C ₁)			G ⁺ G ⁻ (C ₁)		
			calcd freq	PED%	calcd freq	PED%	calcd freq	PED%	calcd freq	PED%	calcd freq	PED%	calcd freq	PED%
2975 (sh)	2971 (vvs)	2954	S19(49), S38(35), S28(15)	S19(89)	2955	S19(89)	2964	S38(64), S19(20), S28(13)	2966	S38(46), S37(35), S28(11)	2975	S37(62), S38(33)	2979	S19(90)
		2969	S38(58), S28(30)	S37(50), S38(37), S28(7)	2967	S37(50), S38(37), S28(7)	2973	S37(96)	2979	S19(70), S28(21), S38(7)	2979	S19(90)	2988	S3(99)
		2974	S19(11), S37(98)	S38(49), S37(46)	2980	S38(49), S37(46)	2989	S3(99)	3024	S2(97)	3024	S2(97)	3024	S2(97)
		3000 (s)	S3(99)	S3(99)	2988	S3(99)	2989	S3(99)						
		3020 (s)	S2(98)	S2(98)	3023	S2(98)	3024	S2(97)						
		3200 (vs)												
		3460 (s)												

^aCombination band. ^bOvertone band.

(calculated at 338 cm⁻¹ for the G⁺T form), ~490 cm⁻¹ (calculated at 465 cm⁻¹ for the G⁺T form), and ~629 cm⁻¹ (calculated at 624 cm⁻¹ for the G⁺T form). Among them, the 490 and 629 cm⁻¹ bands also appear as distinct and strong signals in the IR spectrum. The 345 and 490 cm⁻¹ bands are attributed to $\rho(O-C-O)$ rocking and $\delta(C-O-C)$ deformation, while the 629 cm⁻¹ band is shown to have dominant contributions from $\beta(C-O-C)$ bending and $\nu(C-C)$ stretching vibrations stemming from the G⁺T rotameric form of the molecule. Apart from these, the 1085 cm⁻¹ (calculated at 1082 cm⁻¹ for the G⁺T form) band, which appears as a medium-strong signal in the IR spectrum but is absent in the Raman spectrum, further corroborates the presence of the G⁺T rotameric form of the PA molecule in the liquid state. However, the existence of both G⁺G⁻ and G⁺T forms of the PA molecule is acknowledged from the appearance of a strong IR band at ~2923 cm⁻¹ (calculated at 2913/2915 cm⁻¹ for the G⁺T/G⁺G⁻ form). This band is assigned to a $\nu_{sym}(CH_2)$ symmetric stretching vibration emanating from either G⁺T or G⁺G⁻ or from both forms of the PA molecule. These data imply the presence of G⁺G⁻ and G⁺T forms of the molecule in the liquid state at room temperature.

An interesting conclusion can be drawn from the vibrational signature centered at ~607 cm⁻¹ (calculated at 605/601 cm⁻¹ for the TT/TG⁺ form). This band exhibits a very strong signal in the IR but appears as a weak shoulder in the RS and has been assigned to have major contribution from the mixed $\beta(O-C-O)$ bending, $\nu(C-C)$ stretching vibrations emanating either from TT or TG⁺ or from both forms of the molecule. This analysis, however, presages the existence of TT and/or TG⁺ forms of the PA molecule.

Normal coordinate analyses further indicate that the vibrational signatures ~1043 cm⁻¹ (calculated at 1040/1038 cm⁻¹ for the TG⁺/G⁺G⁻ form) and ~1021 cm⁻¹ (calculated at 1022/1022 cm⁻¹ for the TT/G⁺T form) are degenerate. The band at ~1043 cm⁻¹ has been assigned to $\nu(C-O)$, $\nu(C-C)$ stretching vibrations stemming from the TG⁺ or G⁺G⁻ form or from both forms of the PA molecule. The ~1021 cm⁻¹ band, which appears as a very strong signal in the FTIR spectrum, has been ascribed to have significant contribution from a $\nu(O-C)$ stretching vibration associated with either TT or G⁺T or from both the forms of the PA molecule in the liquid state.

Interestingly, strong IR signals have been recorded at ~2905 cm⁻¹ (calculated at 2902 cm⁻¹ for the TT form) and ~1077 cm⁻¹ (calculated at 1070 cm⁻¹ for the TG⁺ form). Both of these bands are absent in the RS. The 2905 cm⁻¹ band has been assigned to a $\nu_{sym}(CH_2)$ symmetric stretch, while the 1077 cm⁻¹ band has been assigned to have prominent contributions from mixed $\rho(CH_3)$ rocking and $\nu(C-C)$ stretching vibrations stemming from the TT and TG⁺ forms of the molecule, respectively. The appearance of these bands thus marks the exclusive presence of the TT and the TG⁺ rotameric forms of the PA molecule in the liquid state.

Considerable attention may be further drawn to the medium-intense band centered at ~873 cm⁻¹ (calculated 871/872/870 cm⁻¹ for the TT/TG⁺/G⁺T forms) in the Raman spectrum of the molecule. The band has been primarily ascribed to $\rho(CH_2)$, $\rho(CH_3)$ rocking and $\nu(C-O)$ stretching vibrations stemming from TT/TG⁺/G⁺T, either two or all three rotameric forms of the PA molecule.

The concomitance of TG⁺, G⁺T, G⁺G⁻ and TT, TG⁺, G⁺G⁻ rotamers in either their respective exclusive forms or in pairs are characterized by the presence of vibrational bands at ~1233

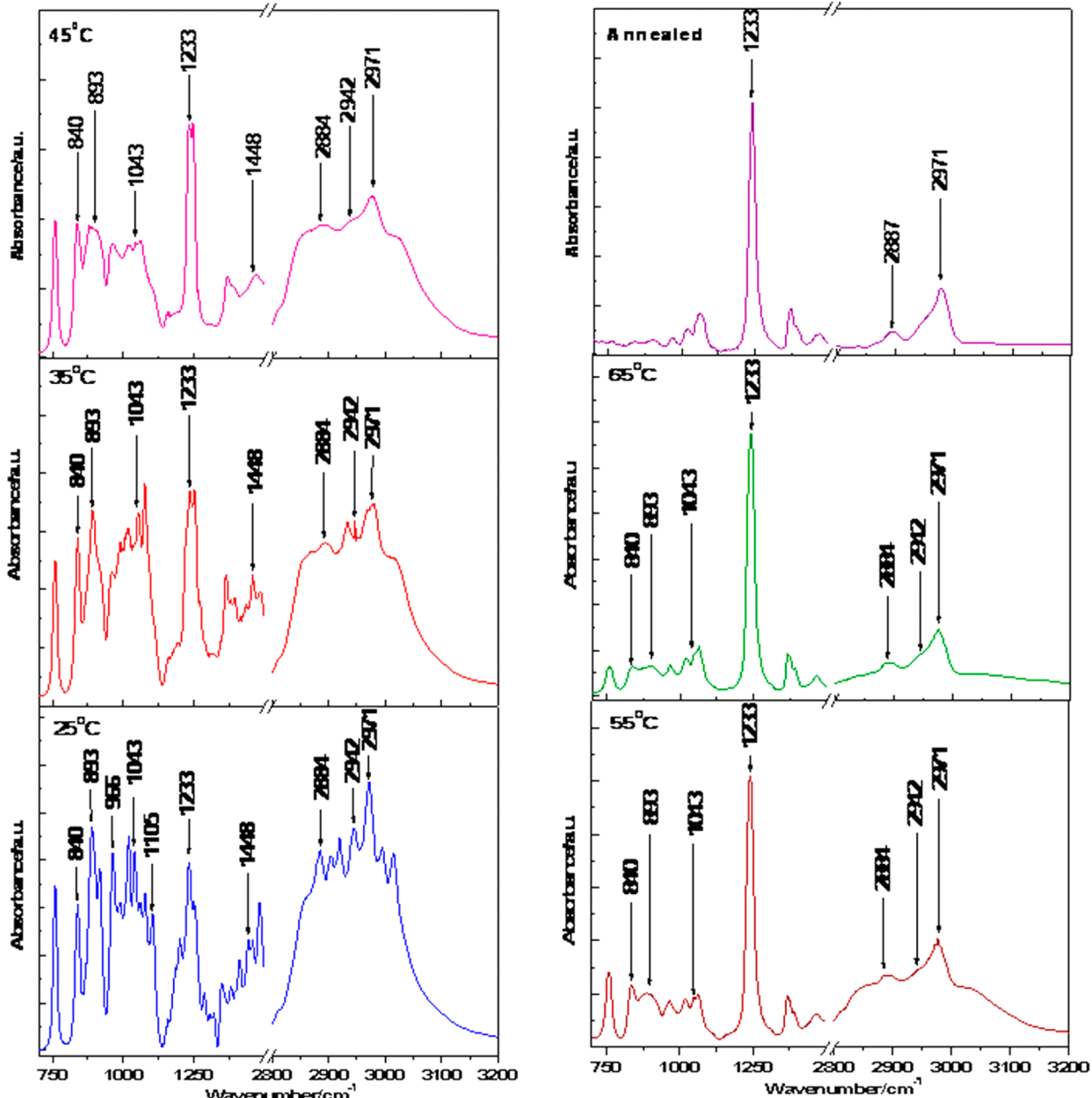


Figure 4. FTIR spectra of the PA molecule in the liquid state recorded at the high-temperature domain ranging from 25 to 65 °C. The upper right panel shows the FTIR spectrum of the annealed sample.

cm^{-1} (calculated at 1237/1224/1227 cm^{-1} for $\text{TG}^+/\text{G}^+\text{T}/\text{G}^+\text{G}^-$ forms) and $\sim 1105 \text{ cm}^{-1}$ (calculated at 1096/1111/1118 cm^{-1} for $\text{TT}/\text{TG}^+/\text{G}^+\text{G}^-$ forms), respectively, in the FTIR spectrum of the molecule recorded in the liquid state.

The presence of TT, TG^+ , G^+T , and G^+G^- forms of the PA molecule is evinced by the appearances of vibrational signatures at $\sim 2942 \text{ cm}^{-1}$ (calculated at 2936/2933/2945/2944 cm^{-1} for $\text{TT}/\text{TG}^+/\text{G}^+\text{T}/\text{G}^+\text{G}^-$ forms), $\sim 2887 \text{ cm}^{-1}$ (calculated at 2885/2886/2883/2885 cm^{-1} for $\text{TT}/\text{TG}^+/\text{G}^+\text{T}/\text{G}^+\text{G}^-$ forms) and $\sim 2975 \text{ cm}^{-1}$ (calculated at 2969, 2974/2967/2973/2975 cm^{-1} for $\text{TT}/\text{TG}^+/\text{G}^+\text{T}/\text{G}^+\text{G}^-$ forms) in the RS and FTIR spectra of the PA molecule in the liquid state at room temperature. Interestingly, strong vibrational signatures centered near 760, 1448, 1462, 1741, and 1774 cm^{-1} in the RS and/or in the IR spectra lack unequivocal assignments from the quantum chemical calculations. The aforementioned bands may emanate from combinations or from overtone vibrational signatures and

are depicted in Table 1. Thus, the above vibrational analyses primarily presage the coexistence of all four rotameric forms (TT, TG^+ , G^+T , and G^+G^-) of the PA molecule in the liquid state at room temperature.

4.3. Temperature-Dependent FTIR Spectra. The FTIR spectra of the PA molecule in the liquid state have been recorded in high- and low-temperature domains to understand its effect on the relative populations of the various rotameric forms. They are shown in Figures 4 and 5, respectively. The FTIR spectra of the molecule recorded in high- and low-temperature domains (Figures 4 and 5) are remarkably different from those recorded at room temperature (25 °C), particularly in the observation window ranges 700–1500 and 2800–3000 cm^{-1} . An increase in temperature (from 25 to 65 °C) results in significant variations in the relative intensities of the bands centered near 1233 and 2971 cm^{-1} with concomitant decreases in the intensities of the 607, 630, 840, 1043, 1448,

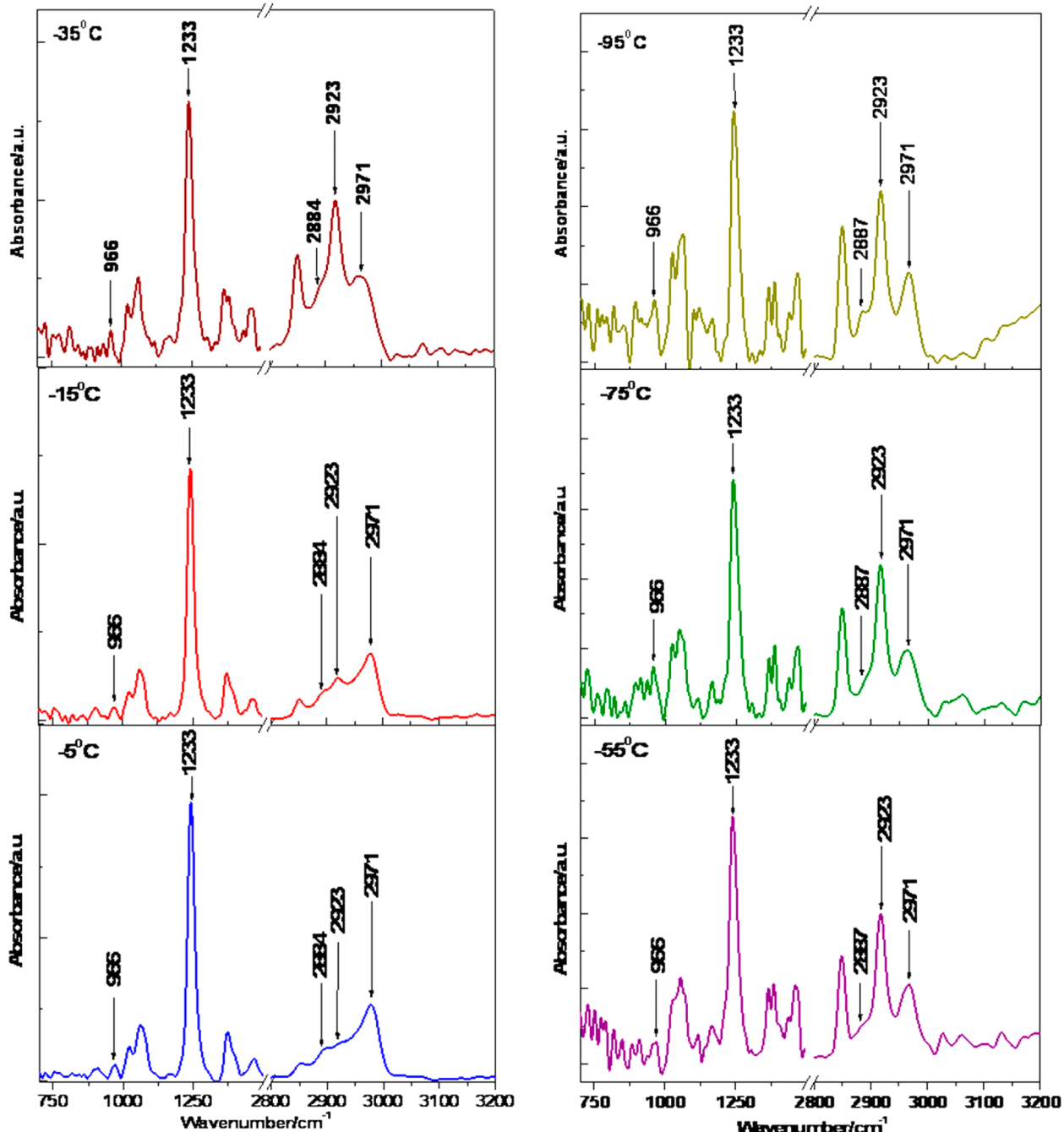


Figure 5. FTIR spectra of the PA molecule in the liquid state recorded at low temperatures ranging from -5 to -95 $^{\circ}\text{C}$.

2884, and 2942 cm^{-1} bands. The variations in the intensities of the 1233 cm^{-1} band (normalized with respect to the well-resolved 1744 cm^{-1} band in the IR spectra) with temperature are shown in the Figure 6b. A significant increase in intensity of the 1233 cm^{-1} band and moderate decrease in intensity of the 2971 cm^{-1} band have been observed with an increase in temperature. The 1233 cm^{-1} band has been assigned to have prevailing contributions from the $\tau(\text{CH}_2)$ twisting vibration stemming from the TG^+ , G^+T , and G^+G^- rotameric forms of the PA molecule. The intensity of this band monotonically increases with an increase in temperature and appears as a sharp intense signal in the FTIR spectra recorded at the high-temperature domain (ca. 55 and 65 $^{\circ}\text{C}$). Interestingly, the other band centered at $\sim 2971\text{ cm}^{-1}$ appears

almost as a sole vibrational signature with a rise in temperature of the PA molecule in the liquid state. This band has been ascribed to $\nu_{\text{asym}}(\text{CH}_3)$ and ν_{antisym} (CH_2); $\nu_{\text{asym}}(\text{CH}_3)$ stretching vibrations emanating from the TT ; TG^+ , G^+T , G^+G^- rotameric forms of the molecule. The annealed IR spectrum, as shown in Figure 4, is also marked by sharp and distinct vibrational signatures centered near 1233 and 2971 cm^{-1} . The variations in the relative intensities of the vibrational signatures with temperature may primarily signify alterations in populations of various rotameric forms of the molecule in the liquid and in the annealed state. However, these vibrational signatures may be degenerate or may represent an exclusive rotameric form of the PA molecule, although this is difficult to deconvolute from the spectral features.

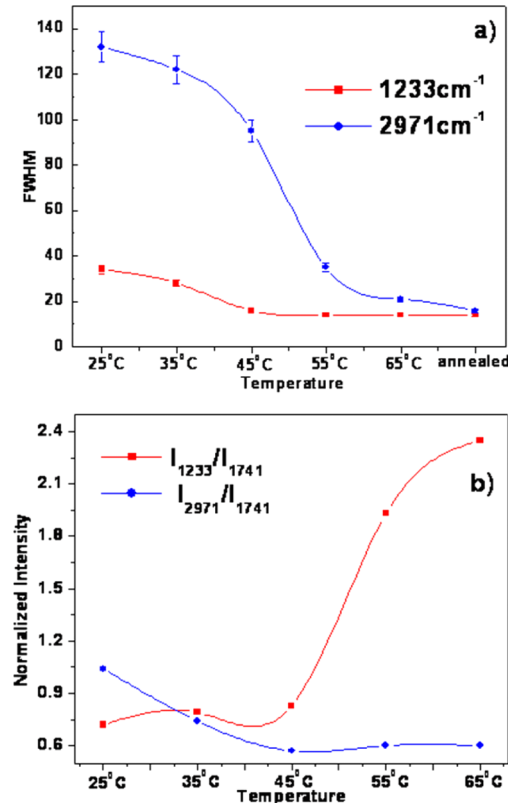


Figure 6. (a) Variations in fwhm of 1233 and 2971 cm^{-1} bands (b) Variations in the normalized intensities of 1233 and 2971 cm^{-1} bands with temperature in the high-temperature domain.

Figure 6a shows the variations in the fwhm of the aforementioned bands with temperature. The fwhm values of these bands, as obtained from the annealed spectrum, are also shown in the same figure (Figure 6a). The significant decrease in the fwhm of the 2971 and 1233 cm^{-1} bands with a rise in temperature may primarily indicate the exclusive presence of a specific rotameric form of the PA molecule in the liquid state, particularly in the high-temperature domain ($>55\text{ }^{\circ}\text{C}$). The annealed spectrum also gives a similar observation.

FTIR spectra of the PA molecule in the low-temperature domain (ca. -5 to $-95\text{ }^{\circ}\text{C}$) are remarkably different in comparison to those recorded at room or at high temperatures. The normalized intensities (normalized with respect to the $1744\text{ } \text{cm}^{-1}$ band) of the 1233 and 2971 cm^{-1} bands increase with a decrease in temperature, attain their respective maximum values near $-25\text{ }^{\circ}\text{C}$, and then decrease again with a further decrease in temperature. The variations are shown in Figure 7b. The temperature-dependent IR spectra are also marked by the distinct appearances of vibrational signatures centered at ~ 2923 and $2971\text{ } \text{cm}^{-1}$. The 2923 and 2971 cm^{-1} bands are assigned to $\nu_{\text{sym}}(\text{CH}_2)$ symmetric and $\nu_{\text{asym}}(\text{CH}_3)$, $\nu_{\text{antisym}}(\text{CH}_2)$; $\nu_{\text{asym}}(\text{CH}_3)$ stretching vibrations emanating from the G⁺T, G⁺G⁻ and TT; TG⁺, G⁺T, G⁺G⁻ forms of the PA molecule, respectively. The appearance of these bands marks the presence of TG⁺, G⁺T, and G⁺G⁻ rotameric forms of the molecule at the low-temperature domain. The fwhm values of the 1233 and 2971 cm^{-1} bands have also been estimated, and their variations in the low-temperature domain are shown in Figure 7a. The fall in fwhm of 1233 and 2971 cm^{-1} on and from $-15\text{ }^{\circ}\text{C}$ may also presage the existence of an exclusive rotameric form of the PA molecule at the low-temperature domain.

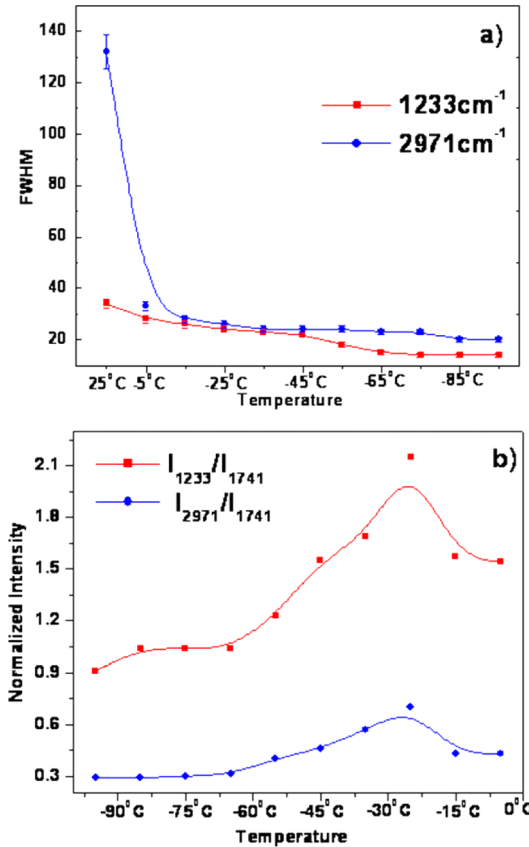


Figure 7. (a) Variations in fwhm values of 1233 and 2971 cm^{-1} bands. (b) Variations in the normalized intensities of 1233 and 2971 cm^{-1} bands with temperature in the low-temperature domain.

The above experimental observations thus allow us to refine the vibrational signatures of 1233 and 2971 cm^{-1} bands. The significant decrements in the fwhm values of the aforementioned bands with the rise and fall in temperatures may indicate the exclusive presence of the TG⁺ rotameric form of the PA molecule in these temperature domains. The 1233 and 2971 cm^{-1} bands have been ascribed to $\tau(\text{CH}_2)$ twisting and $\nu_{\text{asym}}(\text{CH}_3)$ stretching vibrations emanating exclusively from the TG⁺ rotameric form of the PA molecule. The predominance of the TG⁺ form of the PA molecule at low and high temperatures may be related to the barrier energetics concerning the interplay among structural ($\Delta E_{\text{structural}}$), hyperconjugation ($\Delta E_{\text{delocalization}}$), and steric (ΔE_{steric}) energy changes.^{26–28} Understanding the barrier energetics of the PA molecule in detail at high and low temperatures is indeed an interesting field of study, to be considered in a separate publication.

4.4. Car-Parrinello Molecular Dynamics Simulation Study. To understand the preferential existence of the various rotameric forms of the PA molecule at various temperature domains (ca. 65, 25, and $-95\text{ }^{\circ}\text{C}$), CPMD simulations have been performed. The time evolutions of the relevant dihedral angles C₂—O₃—C₄—C₅ (φ_1) and O₃—C₄—C₅—C₆ (φ_2) of the PA molecule have been estimated. The trans (T) and gauche (G^{+/G⁻) forms of the PA molecule are represented by φ_i ($i = 1, 2$) values of 180 and $\pm 60^{\circ}$, respectively. Figure 8 shows the time evolution of the dihedral angles (φ_1, φ_2) of the PA molecule simulated at high ($65\text{ }^{\circ}\text{C}$), room ($25\text{ }^{\circ}\text{C}$), and low temperatures ($-95\text{ }^{\circ}\text{C}$). The superimposed time series plots, as shown in Figure 8, depict the synergetic variations of the}

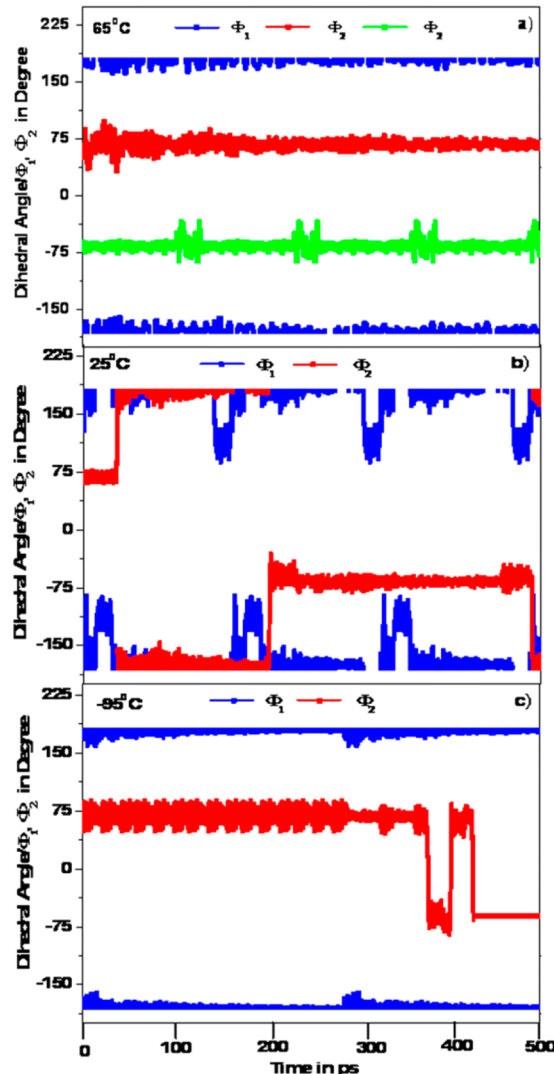


Figure 8. Variation of the superimposed dihedral angles ϕ_1 ($C_2-O_3-C_4-C_5$) and ϕ_2 ($O_3-C_4-C_5-C_6$) of the PA molecule with time as estimated from Car-Parrinello molecular dynamics studies simulated at (a) 65 °C, (b) 25 °C, and (c) -95 °C.

dihedral angles ϕ_1 and ϕ_2 of the PA molecule at the aforementioned temperatures. The variations of ϕ_1 are characterized by distinct crests and troughs, while ϕ_2 exhibits distinct jumps over a 500 ps time scale at 25 °C (Figure 8b). The time series plots, as shown in Figure 8b, thus mark the concomitance of TT, TG⁺, G⁺T, and G⁺G⁻ forms of the PA molecule at room temperature (25 °C). The discrete snapshots of the MD simulations captured at various picosecond time scales are shown in Figure 9 to indicate the existence of TT, TG⁺, G⁺T, and G⁺G⁻ forms of the PA molecule at room temperature (25 °C). However, the time evolutions of the related dihedral angles for the PA molecule at high and low temperatures (65 and -95 °C) are markedly different from those estimated at room temperature.

The variations of the dihedral angles ϕ_1 and ϕ_2 for the PA molecule simulated at high (ca. 65 °C) and at low temperatures (ca. -95 °C) are shown in parts a and c of Figure 8, respectively. The superimposed plot thus marks the presence of TG⁺ and its enantiomeric TG⁻ form of the PA molecule at 65 °C. Interestingly, the time series plot of the dihedral angle ϕ_1 of the PA molecule at low temperature (ca. -95 °C) generates an

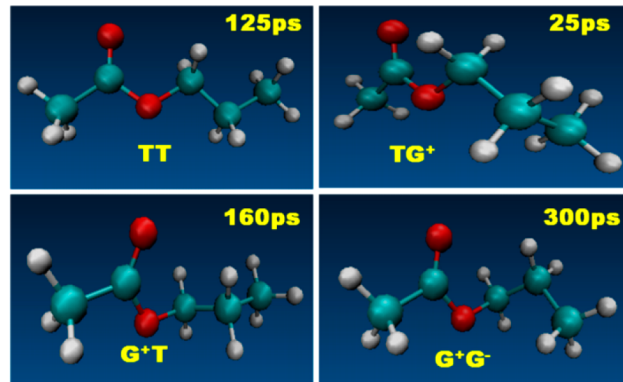


Figure 9. Snapshots of the molecular dynamics simulations captured at various picosecond time scales of the PA molecule at room temperature.

almost smooth signature, indicating the presence of the T form of the PA molecule. The plot is shown in Figure 8. However, the time evolutions of the other dihedral angle ϕ_2 shows similar flat progressions followed by distinctive wells, characteristic of the G⁺ and G⁻ forms of the PA molecule. The superimposed plots of these two dihedral angles ϕ_1 and ϕ_2 also signify the existence of TG⁺ and TG⁻ forms of the PA molecule at -95 °C. Thus, in general the superimposed time series plots, as shown in Figure 8a,c, both mark the presence of TG⁺ forms of the PA molecule at high and low temperatures (65 and -95 °C). The corresponding snapshots, depicting the possible existence of the TG⁺ form of the molecule at high and low temperatures (65 and -95 °C), are shown in Figure 10. The

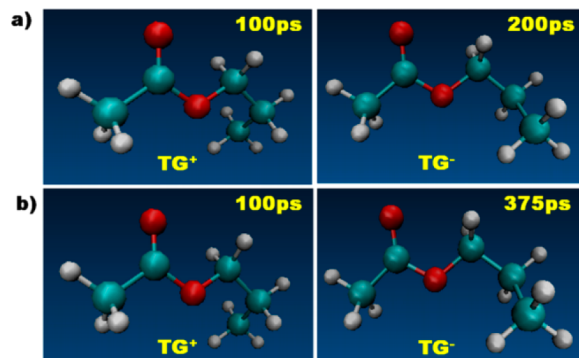


Figure 10. Snapshots of the molecular dynamics simulations captured at various picosecond time scales of the PA molecule at (a) high temperature and (b) low temperature.

preferential existence of the TG⁺ form at low and high temperatures, as estimated from the CPMD simulations, may further allow us to refine the vibrational signature of the rotameric forms of the PA molecule obtained from quantum chemical calculations. The vibrational signatures ~ 1233 and 2971 cm^{-1} in the high- and low-temperature domains may now be considered to emanate exclusively from the TG⁺ rotameric form of the PA molecule. The dramatic decrements of fwhm of the aforementioned bands also support the above conjecture. The results of CPMD simulations are thus correlated with the experimentally observed FTIR spectra and their corresponding analyses aided by ab initio quantum chemical calculations.

In this connection it may be mentioned that CPMD simulations further suggest that the barrier height between

TG^+ and TG^- forms of the PA molecule increases with increasing temperature. To understand the origin of this barrier height, explicit partition of the total energy changes (ΔE) into energy changes related to the structural ($\Delta E_{\text{structural}}$), hyperconjugation ($\Delta E_{\text{delocalization}}$), and steric energies (ΔE_{steric}) with temperature have to be considered in detail. The interactions between the ester and methyl groups of the PA molecule result in torsion potential which may change with an increase in temperature. Understanding the origin of the barrier height between TG^+ and TG^- forms of the molecule with changes in temperature is indeed an interesting aspect and will be detailed in a separate publication.

5. CONCLUSION

The conformational preferences of various rotameric forms of propyl acetate (PA) molecules have been investigated from the Raman and FTIR spectra, aided by ab initio quantum chemical and Car–Parrinello molecular dynamics simulation studies. Using the MP2/aug-cc-pVTZ level of theory, the optimized structural parameters of all the different rotameric forms of the PA molecule have been estimated. The vibrational modes of the PA molecule have been assigned for the first time on the basis of potential energy distributions (PEDs). The vibrational signatures, as obtained from the Raman and temperature dependent FTIR, envisage the concomitance of TT, TG^+ (TG^-), G^+T (G^-T), and G^+G^- (G^-G^+) rotameric forms of the PA molecule at room temperature. However, at low (ca. -95°C) and high temperatures (ca. 65°C), the TG^+ (enantiomeric TG^-) form of the PA molecule is predominant. These results are obtained from the Car–Parrinello molecular dynamics (CPMD) simulations in conjunction with the analyses of fwhm values of some imperative vibrational signatures of the molecule. CPMD simulations together with the temperature-dependent IR spectroscopic studies thus help to decipher the exclusive presence of the TG^+ rotameric form of the PA molecule at low and high temperatures.

■ ASSOCIATED CONTENT

Supporting Information

Selected optimized structural parameters, dipole moments, and rotational constants (Table S1), definition of internal and local symmetry coordinates of the EP molecule (Table S2), intensity profile of Raman bands as obtained from experimental and theoretical considerations (Figure S3), and vibrational frequencies at ~ 1233 and 2971 cm^{-1} which mark the exclusive presence of the TG^+ form of the molecule at high and low temperatures (Table S4). The Supporting Information is available free of charge on the ACS Publications website at DOI: 10.1021/acs.jpca.5b03486.

■ AUTHOR INFORMATION

Corresponding Author

*J.C.: e-mail, joydeep72_c@rediffmail.com; tel, (033) 24624554; fax, (033)24626869.

Notes

The authors declare no competing financial interest.

■ ACKNOWLEDGMENTS

J.C. thanks the DAE-BRNS, DST, Government of India, for financial support through Research Projects (Project Nos. 2012/37P/27/BRNS/ and SR/S2/CMP-0045/2012). J.C. also thanks his bon2 (sister) Mrs. Uma Banerjee for engrossing the

mind in the world of fragrances and identifying the molecular behavior behind it.

■ REFERENCES

- Jenner, P. M.; Hagan, E. C.; Taylor, J. M.; Cook, E. L.; Fitzhugh, O. G. Food Flavourings and Compounds of Related Structure I. Acute Oral Toxicity. *Food Cosmet. Toxicol.* **1964**, *2*, 327–343.
- Gustavsson, A.; Larsson, M. C.; Hansson, B. S.; Liljefors, T. Enantiomers of Cis- and Trans-3-(4-propyl-cyclopent-2-enyl) Propyl Acetate. A Study on the Bioactive Conformation and Chiral Recognition of a Moth Sex Pheromone Component. *Bioorg. Med. Chem.* **1997**, *5*, 2173–2183.
- Ogawa, Y.; Tasumi, M. Raman and Infrared Spectroscopic Studies on Conformational Polymorphism of N – Propyl Acetate. *Chem. Lett.* **1979**, 1411–1412.
- Dutta, B.; Tanaka, T.; Banerjee, A.; Chowdhury, J. Conformational Preferences of Ethyl Propionate Molecule: Raman, Temperature Dependent FTIR Spectroscopic Study Aided by *Ab Initio* Quantum Chemical and Car–Parrinello Molecular Dynamics Simulation Studies. *J. Phys. Chem. A* **2013**, *117*, 4838–4850.
- Lawson Daku, L. M.; Linares, J.; Boillot, M. *Ab initio* Static and Molecular Dynamics Study of 4 Styrylpyridine. *ChemPhysChem* **2007**, *8*, 1402–1416.
- Frisch, M. J.; Trucks, G. W.; Schlegel, H. B.; Scuseria, G. E.; Robb, M. A.; Cheeseman, J. R.; Montgomery, J. A., Jr.; Vreven, T.; Kudin, K. N.; Burant, J. C.; et al. *Gaussian 09*; Gaussian, Inc., Pittsburgh, PA, 2009.
- Møller, C.; Plesset, M. S. Note on an Approximation Treatment for Many-Electron Systems. *Phys. Rev.* **1934**, *46*, 618–622.
- Merrick, J. P.; Moran, D.; Radom, L. An Evaluation of Harmonic Vibrational Frequency Scale Factors. *J. Phys. Chem. A* **2007**, *111*, 11683–11700.
- Wilson, E. B.; Decius, J. C.; Cross, P. C. *Molecular Vibrations: The Theory of Infrared and Raman Vibrational Spectra*; McGraw-Hill: New York, 1955.
- Kuwae, A.; Machida, M. The CH Out-of-Plane Deformation Vibrations of Monosubstituted Benzenes and Effect of Substituents on Related Force Constants. *Spectrochim. Acta. Part A* **1978**, *34*, 785–791.
- CPMD; IBM Corp. 1990–2008; MPI für Festkörperforschung Stuttgart 1997–2001; <http://www.cpmd.org/> (accessed May 18, 2013).
- Nose, S. A. A Unified Formulation of the Constant Temperature Molecular Dynamics Methods. *J. Chem. Phys.* **1984**, *81*, 511–519.
- Hoover, G. Canonical dynamics: Equilibrium Phase-Space Distributions. *Phys. Rev. A: At., Mol., Opt. Phys.* **1985**, *31*, 1695–1697.
- Perdew, J. P.; Burke, S.; Ernzerhof, M. Generalized Gradient Approximation Made Simple. *Phys. Rev. Lett.* **1996**, *77*, 3865–3868.
- Troullier, N.; Martins, J. L. Efficient Pseudopotentials for Plane-Wave Calculations. *Phys. Rev. B: Condens. Matter Mater. Phys.* **1991**, *43*, 1993–2006.
- Humphrey, W.; Dalke, A.; Schulten, K. VMD: Visual Molecular Dynamics. *J. Mol. Graphics* **1996**, *14*, 33–38.
- Chun, H. J.; Meinander, N.; Villarreal, J. R.; Laane, J. Vibrational Spectra, Theoretical Calculations and Two-Dimensional Potential Energy Surface for the Ring-Puckering Vibrations of 2,4,7-Trioxa[3.3.0]octane. *J. Phys. Chem. A* **2015**, *119*, 410–417.
- Chandra, S.; Chowdhury, J.; Ghosh, M.; Talapatra, G. B. Genesis of Enhanced Raman Bands in SERS Spectra of 2-Mercaptoimidazole: FTIR, Raman, DFT, and SERS. *J. Phys. Chem. A* **2012**, *116*, 10934–10947.
- Chowdhury, J.; Chandra, S.; Ghosh, M. Adsorption and Trace Detection of Pharmacologically Significant 5-Methylthio-1, 3, 4-Thiadiazole-2-Thiol Molecule Adsorbed on Silver Nanocolloids and Understanding the Role of Albrecht's “A” and Herzberg-Teller Contributions in the SERS Spectra. *Spectrochim. Acta, Part A* **2015**, *135*, 935–946.
- Pande, S.; Chowdhury, J.; Pal, T. Understanding the Enhancement Mechanisms in the Surface-Enhanced Raman Spectra

of the 1,10-Phenanthroline Molecule Adsorbed on a Au@Ag Bimetallic Nanocolloid. *J. Phys. Chem. C* **2011**, *115*, 10497–10509.

(21) Chandra, S.; Chowdhury, J.; Ghosh, M.; Talapatra, G. B. Adsorption of 3-Thiophene Carboxylic Acid on Silver Nanocolloids: FTIR, Raman and SERS Study Aided by Density Functional Theory. *J. Phys. Chem. C* **2011**, *115*, 14309–14324.

(22) Aroca, R. F.; Clavijo, R. E.; Halls, M. D.; Schlegel, H. B. Surface-Enhanced Raman Spectra of Phthalimide. Interpretation of the SERS Spectra of the Surface Complex Formed on Silver Islands and Colloids. *J. Phys. Chem. A* **2000**, *104*, 9500–9505.

(23) Bolboaca, M.; Iliescu, T.; Paizs, Cs.; Irimie, F. D.; Kiefer, W. Raman, Infrared and Surface-Enhanced Raman Spectroscopy in Combination with *Ab Initio* and Density Functional Theory Calculations on 10-Isopropyl-10Hphenothiazine- 5-oxide. *J. Phys. Chem. A* **2003**, *107*, 1811–1818.

(24) Chandra, S.; Chowdhury, J.; Ghosh, M.; Talapatra, G. B. Genesis of Enhanced Raman Bands in SERS Spectra of 2-Mercaptoimidazole: FTIR, Raman, DFT and SERS. *J. Phys. Chem. A* **2012**, *116*, 10934–10947.

(25) Lapinski, L.; Nowak, M. J.; Kwiatkowski, J. S.; Leszczynski. Phototautomeric Reaction, Tautomerism and Infrared Spectra of 6-Thiopurine. Experimental Matrix Isolation and Quantum-Mechanical (Conventional *Ab Initio* and Density-Functional Theory) Studies. *J. Phys. Chem. A* **1999**, *103*, 280–288.

(26) Dutta, B.; De, R.; Pal, C.; Chowdhury, J. Vibrational analysis of the Conformers and Understanding the Genesis of the Internal Rotational Barriers of Isobutyl Cyanide Molecule. *Spectrochim. Acta, Part A* **2012**, *96*, 837–847.

(27) Dutta, B.; De, R.; Chowdhury, J. *Ab initio* and DFT study to Understand the Physics Behind the Conformational Barriers of Isobutyl Cyanide Molecule. *Indian J. Phys.* **2013**, *87*, 855–863.

(28) Dutta, B.; Chowdhury, J. Origins of Threelfold Rotational Barriers of Molecule Containing Two Methyl Groups: Ethyl propionate as Paradigm. *Chem. Phys. Lett.* **2014**, *612*, 89–96.